Energy Level and Band Alignment for GaAs−Alkylthiol Monolayer−Hg Junctions from Electrical Transport and Photoemission Experiments

Guy Nesher, Ayelet Vilan, Hagai Cohen, and David Cahen*

Weizmann Institute of Science, Rehovoth, Israel

Fabrice Amy, Calvin Chan, Jaehyung Hwang, and Antoine Kahn

Department of Electrical Engineering, Princeton University, Princeton, New Jersey

Received: April 7, 2006; In Final Form: May 22, 2006

A series of *p*- and *n*-GaAs−S−C$_n$H$_{2n+1}$ || Hg junctions are prepared, and the electronic transport through them is measured. From current−voltage measurements, we find that, for *n*-GaAs, transport occurs by both thermionic emission and tunneling, with the former dominating at low forward bias and the latter dominating at higher forward bias. For *p*-GaAs, tunneling dominates at all bias voltages. By combining the analysis of the transport data with results from direct and inverse photoemission spectroscopy, we deduce an energy band diagram of the system, including the tunnel barrier and, with this barrier and within the Simmons tunneling model, extract an effective mass value of $1.5−1.6m_e$ for the electronic carriers that cross the junctions. We find that transport is well-described by lowest unoccupied and highest occupied states at $1.3−1.4$ eV above and $2.0−2.2$ eV below the Fermi level. At the same time, the photoemission data indicate that there are continua of states from the conduction band minimum and the valence band maximum, the density of which varies with energy. On the basis of our results, it appears likely that, for both types of junctions, electrons are the main carrier type, although holes may contribute significantly to the transport in the *p*-GaAs system.

1. Introduction

Can we measure and understand the electrical transport properties of a single layer of molecules placed between two solid electrodes? Only if we can answer this question can we hope to be able to predict the behavior of new systems and assess their potential for practical implications as molecular junctions. However, measuring such systems poses serious challenges. To meet these challenges, we need to design systems that allow measurement of the relevant properties in a reliable and reproducible fashion.

To date, most of the work in this field has been performed on metal/molecules/metal junctions with the molecules chemically or physically adsorbed to one (or both) of the metal electrodes.[1,2] We choose to use a semiconductor as one of the electrodes because of a number of advantages, such as the ability to change the work function of the electrode without changing the nature of the chemical bond. Earlier work with semiconductor/molecules/metal junctions can be found in refs 3−5 for Si, and in refs 6 and 7 for GaAs.

Conjugated molecules with a small energy gap between the highest occupied and lowest unoccupied molecular orbitals are often studied in molecular junctions. Here we choose to use alkyls, that is, large-gap saturated molecules. While it is easy to justify the use of saturated molecules (most molecules are not conjugated, and thus the results can be of broader importance), the main reason for our choice is that these molecules are relatively simple, and their investigation may help to reveal the fundamental mechanisms of electronic transport across molecules with *localized* electronic states.

The nature of contacts is a critical issue in molecular junctions. In the case of self-assembled monolayers, one contact can be made by chemi- or physisorption of the molecules onto a conducting substrate. Making a junction then requires a second contact, which should be made in a nondestructive, noninvasive manner. Methods such as lift-off float-on (LOFO),[8] nanotransfer printing,[6] direct metal evaporation on molecules with sacrificial headgroups,[9] or indirect metal evaporation on the molecules[10] have been developed to make that top contact. In addition to these methods, a liquid mercury electrode provides a simple alternative for laboratory use. The very high surface tension of liquid metals limits the ability of Hg to penetrate into monolayer defects, including pinholes, thus avoiding shorting via pinholes.[11,12] As a result, excellent reproducibility can be achieved as long as the Hg surface is not contaminated by the ambient.

We recently reported the electrical transport characteristics of a series of *n*-Si/alkyl/Hg systems for alkyl lengths systematically varied from 12 to 18 carbon atoms. From analyses of the transport and photoelectron spectroscopic data, we concluded that electronic transport through those junctions is limited by thermionic emission over a barrier in the Si at low forward bias, and by tunneling through the molecular barrier at higher bias. At low bias, the thermionic emission barrier is largest and dictates transport, while, at higher bias, the thermionic emission barrier is reduced so much that the tunneling barrier dictates transport. Because these results, while being in agreement with predictions for metal−insulator−semiconductor (MIS) junctions,[13] differ from earlier reported results with Si,[3,4] it is of direct interest to see whether GaAs junctions of this type show similar behavior or yield results that are more similar to those of earlier reports.[6,7]

Monolayers of alkylthiols on GaAs have been studied at least since Sheen et al.[14] used them over a decade ago. Since then, more research has been performed[15−19] on the quality of the

---

* Corresponding author.

monolayers and their electrical properties, mostly using one specific alkylthiol, that is, octadecylthiol.

We report the results of our study with a series of rather well-defined monolayers constructed with $CH_3(CH_2)_nSH$ of different chain lengths ($n = 11, 13, 15, 17$; to be referred to as C12, C14, C16, and C18, respectively). We first describe the quality of our monolayers and then show how we gain insight into the transport mechanisms from current–voltage, UV-, as well as inverse photoemission spectroscopic (IPES) data.

2. Experimental Section

GaAs. (100) wafers, n-doped Si at $1.2-1.3 \times 10^{18}$ cm^{-3} and p-doped Zn at $2.5-2.6 \times 10^{18}$ cm^{-3} were purchased from AXT (CA). The GaAs substrates were cleaned by sonication, sequentially in 2-propanol, acetone, and methanol, 10 min for each solvent, followed by ozone oxidation for 25 min in a UVOCS apparatus. The oxide was removed by a 5 s dip in 2% hydrofluoric acid, a rinse in water, then a 30 s dip in diluted NH_4OH (1:9) followed by a rinse in water again.[20–23] After drying in a stream of dry N_2, the sample was immediately placed in the adsorption solution. The surface roughness, as determined by atomic force microscopy (AFM), was found to be 0.6 nm ($\pm$0.2 nm).

Chemicals. 1-Dodecanethiol (>98%), 1-tetradecanethiol (>98%), and 1-octadecanethiol (>98%) were purchased from Aldrich. 1-Hexadecanethiol (>95%) was purchased from Fluka. The thiols were used without further purification. All the chemicals were used without further purification. Deionized water was used (18 MΩ).

Adsorption. The molecules self-assembled on the GaAs substrate from a 5 mM methanol solution. After placing the samples in the solution (immediately after etching), the adsorption solution was heated for 5 min to 50 °C and then placed in a N_2 atmosphere for 3 min. From the N_2 atmosphere, the samples were transferred to a desiccator for overnight adsorption. After adsorption, the samples were rinsed in methanol.

Contact-Angle Measurements. Static contact-angle measurements were performed with an automated goniometer (Rame-Hart, model 100). Approximately 4 μL of deionized water (Millipore, Inc.) was deposited onto the sample using a microsyringe. Measurements were recorded immediately after deposition.

Ellipsometry. The layer thickness was deduced from ellipsometry, using an M 2000V (J. A. Wollam Co., Inc.) spectroscopic ellipsometer with a spectral range from 370 to 1000 nm. The data were fit using Wvase32 software. We used a Cauchy model for the top organic layer with $a = 1.45$, $b = 0.01$, and $c = 0$.

Fourier Transform Infrared (FTIR). The measurements were performed on a Bruker EQUINOX-55 in the transmission mode, using a liquid nitrogen-cooled mercury cadmium telluride (MCT) detector. The spectra were corrected for background by subtracting a reference spectrum obtained from a cleaned and etched GaAs sample.

X-ray Photoelectron Spectroscopy (XPS). At the Weizmann Institute, measurements were performed on a Kratos Analytical AXIS-HS instrument, using a monochromatized Al Kα (1486.6 eV) source at a relatively low power (75 W) and a detection pass energy of 20 eV. Ar$^+$ sputtering was applied at 4 keV and a 45° incidence. Composition and thickness analysis was deduced from the O 1s, C 1s, Ga 3d, As 3d and S 2p lines. Ga 2p and As 2p were used for fine identification of sulfide and oxide species, applying curve fitting with Gaussian–Lorentzian line shapes and comparing peak positions to literature data.[15,24–28]
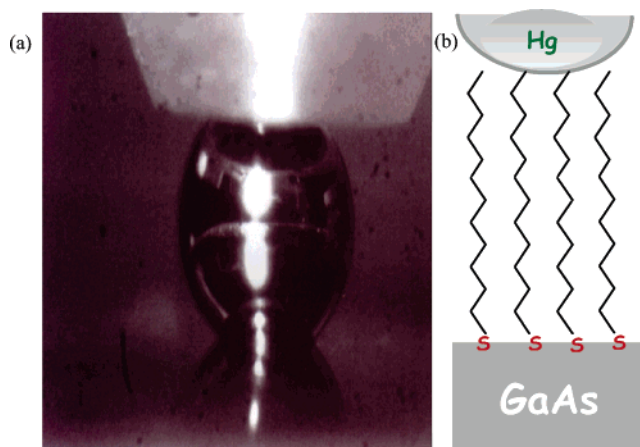
Figure 1. A photograph (a) and an illustration (b) of the junction geometry used here. In panel a, the reflection of the Hg drop in the GaAs wafer is seen in the bottom part of the photograph.
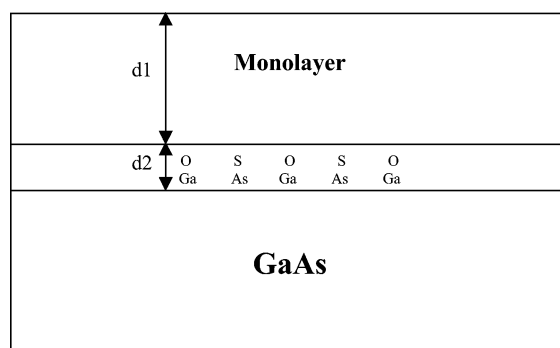
Figure 2. Model used to estimate the thickness of alkylthiol monolayer and oxide on GaAs from XPS data.

XPS thickness analysis corresponds to a model (Figure 2) of a homogeneous organic top layer of thickness d_1 and a thin interfacial layer of thickness d_2, where oxide species (mainly of the Ga) are incorporated between the S atoms that connect the alkyl chains to the GaAs (via As, *vide infra*). Attenuation of the emitted photoelectrons is accounted for by inelastic mean free path (IMFP) parameters of 33 Å for the hydrocarbon and 25 Å for the inorganic layer, neglecting their kinetic energy dependence (across the low binding energy range, up to 550 eV).[29] Layer thicknesses are given by the following expressions:

$$d_1 = \lambda^{\text{org}} \sin \theta \ln\left(\frac{[C]}{[Ga] + [As] + [O]} + 1\right) \quad (1)$$

$$d_2{}^* = \lambda^{\text{inorg}} \sin \theta \ln\left(\frac{[S] + [O]}{[Ga] + [As]} + 1\right) \quad (2)$$

where λ^{org} and λ^{inorg} are the IMFP values of the organic and inorganic matrixes, respectively. Atomic concentrations are given within the square brackets. θ is the takeoff angle with respect to the surface plane. Some uncertainty in the thickness analysis is introduced by the angular broadening of the magnetic lens in the detection system.

UV Photoelectron Spectroscopy (UPS) and XPS. The (molecular monolayer and GaAs) valence band spectra and vacuum level positions were measured at Princeton University with UPS, using He II (40.81 eV) excitation. Given that the GaAs valence band signal is nearly fully attenuated when the molecular monolayer is adsorbed, UPS was complemented by in-situ XPS to measure the position of the GaAs valence band

Electron Transport in GaAs−S−C$_n$H$_{2n+1}$−Hg Junctions

J. Phys. Chem. B, Vol. 110, No. 29, 2006 **14365**

maximum with respect to the Fermi level and thus the band bending in the semiconductor with the molecular overlayer. Al Kα (1486.6 eV) and Zr Mζ (151.4 eV) were used for different surface sensitivities. The Ga3d and As3d core levels and valence band of the clean (sputtered and annealed) GaAs surface were measured independently to establish the precise energy differences between the 3d core levels and the valence band maximum. The core level positions were then measured on the monolayer-covered GaAs and used to establish the band bending. Careful decomposition of the core levels was performed to distinguish Ga−As from the Ga−O and As−S bonds. The numbers given correspond to the positions of the centers of the Gaussian peaks used for decomposition. The position of the Fermi level was measured via UPS on a clean film of Au. The overall instrumental resolution in UPS, measured from the Au Fermi step, was 150 meV.

Inverse Photoemission Spectroscopy (IPES). IPES was performed in the isochromat mode, using a fixed-energy photon detector[30] and a low energy electron gun. The overall IPES instrumental resolution, estimated from the width of the Fermi edge measured on Ta, was 450 meV. The primary electron current density was held below 1 μA/cm².

Current (Density)−Voltage (J−V) Measurement. The Hg drop setup is described elsewhere.[31] Current−voltage (J−V) characteristics were collected in a voltage scan mode, using an HP 4155 semiconductor parameter analyzer. The bias polarity convention is that the voltage is positive for junctions on p-type wafers if the wafer's back-contact is positive, and for junctions with n-type wafers if the Hg drop is positive.

We used several scan rates and monitored the stability of the junction and the deterioration of the monolayer. The J−V curves that are shown are always those obtained from the first measurement of the junction. Subsequent measurements, performed without lifting the Hg drop or making any other changes, led to a current increase, apparently due to monolayer defects that were introduced during the first J−V scan. There are several reasons for this. The lateral mobility of thiols on GaAs is high, and thus the bias, if not distributed equally, may move them and create pinholes. Furthermore, the As−S bond is rather weak, and hence the thiols may be reduced under electrostatic fields, giving rise to increasing defect concentration.[31] Notwithstanding this complication, the reproducibility of the first measurement for a given sample and from sample to sample was ±10% for currents greater than or equal to 10⁻⁶ A/cm², with a close to 100% error for the lowest currents (10⁻⁸ A/cm²) that could be measured.

Units. Potentials are given in V, from which the electron energies in eV can be obtained by multiplying with the electron charge q.

3. Results

Monolayer Properties. *Ellipsometry.* In ellipsometry measurements, surface roughness generally limits the ability to deduce the *absolute* thickness of an organic monolayer with an estimated width of a few nanometers on a GaAs surface.[14] However, using this method to compare the relative thickness of systems prepared with similar but systematically varied molecules yields more precise (although still relative) data. Here we compare samples made with alkylthiols of different molecular lengths. The measured thicknesses are represented in Table 1 and, as can be seen, the results are comparable to the thickness calculated from XPS measurements (Table 2). These data, and how they can be viewed as absolute numbers, will be discussed below.

TABLE 1: Results of Various Characterizations of Several GaAs−S−C$_n$H$_{2n+1}$ Surfaces

monolayer	ellipsometry thickness (Å) (± 5%)	contact angle (degrees) (±1°)	CH$_2$ antisymmetric stretch peak position (cm⁻¹) from FTIR (± 0.05 cm⁻¹)
C12	14	110	2920.5
C14	19	111	2918.5
C16	21.5	112	2917
C18	24	112	2917

TABLE 2: Thickness Values of the Molecular Layer (d_1) and That Part of the Interfacial Oxide-Containing Film Associated with the S and O Signals Only ($d_2{}^*$),[a] Calculated for Several GaAs−S−C$_n$H$_{2n+1}$ Surfaces, with n = 12, 14, 16, and 18 (See Model Scheme in Figure 2)

| substrate	monolayer	d_1 (Å)[b] (± 10%)	$d_2{}^*$ (Å)[c] (± 50%)
p-GaAs	C12	11.0	2.4
p-GaAs	C14	17.2	1.9
p-GaAs	C16	21.0	2.1
p-GaAs	C18	23.4	2.1
n-GaAs	C16	19.8[d]	1.7
n-GaAs	C18	24.0	2.4
p-GaAs	C12 (oxidized)	7.1	11.2

[a] The total thickness, d_2, is ∼2$d_2{}^*$. [b] d_1 is calculated from eq 1, not including the S signal. [c] $d_2{}^*$ is calculated from eq 2 with S and O, not including the oxidized Ga and As. [d] The experimental error is ±15%.

Contact Angle. The alkyl molecules have hydrophobic tail groups, and the hydrophobicity of the monolayer can be assumed to depend on how closely these tail groups are packed. Sessile drop contact-angle (CA) measurements with water can therefore provide a measure of the monolayer packing density. If one further assumes that the densest packed layers result from the most ordered ones, the CA provides a measure of the monolayer order. The importance of these measurements stems from our experience that a small change in (high) angle for these films can correspond to a significant change in the J−V characteristics. Only samples with contact angles greater than 110° were used for further experiments. Table 1 gives the measured contact angle for the different monolayers.

FTIR. FTIR spectroscopy serves as an additional tool to evaluate the quality of the monolayer. The order of the alkyl chains is reflected in the peak position of the antisymmetric stretch of the methylene groups in the chain.[32] As the antisymmetric stretch moves from 2928 to 2917 cm⁻¹, the monolayer of alkyl chains changes from a liquid to a solid phase. The observed antisymmetric stretch peak positions are reported in Table 1 for the different monolayers. The observed frequencies strongly indicate that the monolayer is densely packed with a low degree of gauche defects. It is also obvious that, generally speaking, better monolayers are formed as the number of carbons in the alkyl chain is increased. This is not surprising, since longer alkyl chains are expected to achieve stronger van der Waals intermolecular interactions and, therefore, improve the order in the monolayer (so as to maximize such interactions, which stabilize the monolayer by ∼6 kJ/methylene/mole). From Table 1, we also conclude that the C14, C16, and C18 monolayers have a more solid-like structure, while the C12 structure is largely disordered.

XPS. Figure 3 compares XPS lines for (1) a p-GaAs−C18 monolayer, (2) a p-GaAs−C12 monolayer, and (3) a p-GaAs−C12 after 4 min of Ar⁺ sputtering. The XPS-derived atomic concentrations indicate only a small amount of surface oxidation, both in terms of O concentration and in terms of oxidized Ga
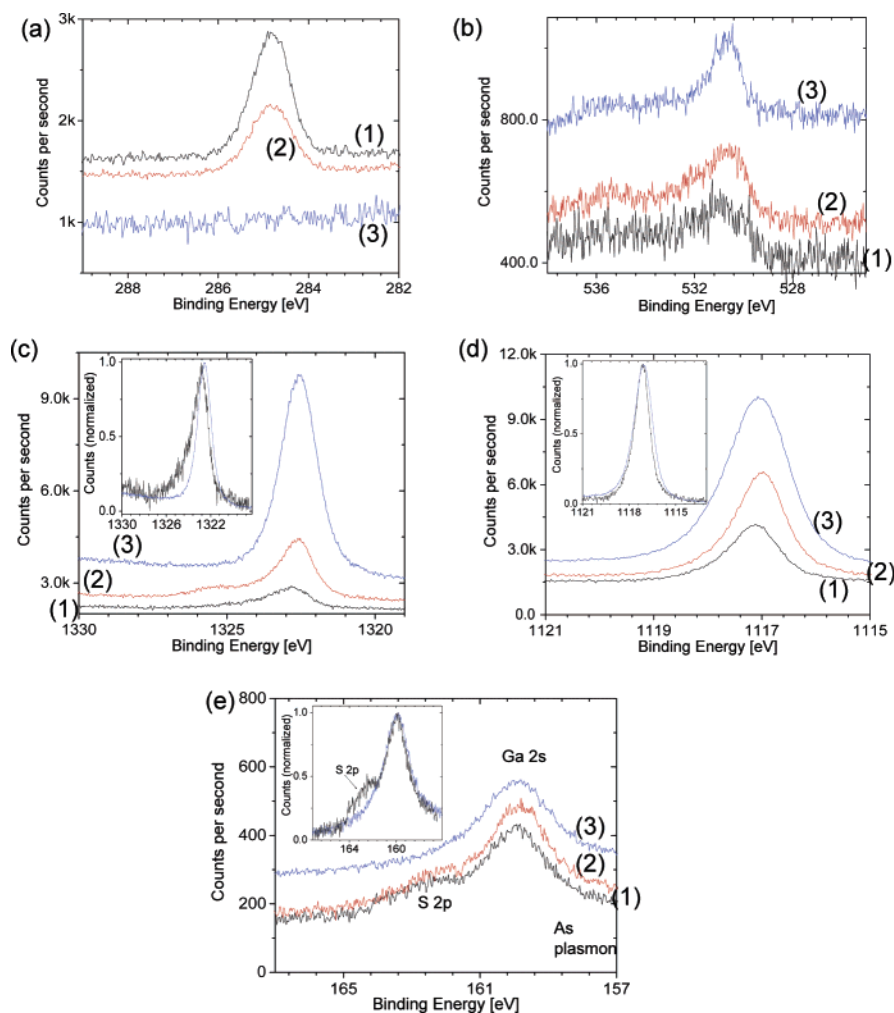
Figure 3. Raw XPS data (shifted vertically for comparison) for a *p*-GaAs−S−C$_n$H$_{2n+1}$ monolayer with $n = 18$ (1/black), $n = 12$ (2/red), $n = 12$, after sputtering (3/blue). (a) C 1s; (b) O 1s; (c) As 2p$_{3/2}$; (d) Ga 2p$_{3/2}$; and (e) S 2p. Insets: Comparison between a $n = 18$ (1/black) and a sputtered $n = 12$ monolayer (3/blue). Curves are normalized.

and As signals. The C 1s peak (Figure 3a) decreases as expected for shorter molecules, with no indication for carbonic contamination. The O 1s line (Figure 3b) overlaps with a Ga Auger signal (∼535 eV) and appears with at least two different oxidation states (e.g., hydroxyls and oxides).

Quantification of the S content (Figure 3e) is limited here because of its spectral overlap with the substrate signals, the Ga2s line (160 eV), and a broad As plasmon feature (∼157 eV). Yet, within our experimental error (∼25% for the S line) and considering photoelectron attenuation corrections, the S signal fits well to the C concentration.

The various oxidation states of As and Ga are better resolved in their 2p$_{3/2}$ lines (panels c and d of Figure 3) than in the 3d lines (which, however, were more suitable for thickness derivation; Table 2). The high binding energy tail of the main As 2p$_{3/2}$ line is attributed mainly to As−S bonds.[15,16] A reference sample was prepared by sputtering a *p*-GaAs−C12 sample and removing the organic layer (see the disappearance of C and S signals in Figure 3a,e, respectively). The O 1s signal does not disappear after the sputtering (Figure 3b), a result that we ascribe to reoxidation during the measurement. Most importantly, no broadening of the As 2p line is observed. Thus, the pronounced broadening of the As 2p signal in the nonsputtered sample should be associated (at least partially) with As−S bonds.

In contrast with the As, the Ga line shape is almost unchanged upon sputtering,[33] suggesting again that the alkylthiol binds

selectively to the substrate through As−S bonds. Our quantitative analysis clearly indicates the existence of oxidized Ga, which is hardly resolvable as a result of its relatively small chemical shift compared to the wafer Ga. Indeed the O to Ga^{ox} ratio is less than or equal to 1, as suggested in Figure 2.

XPS-derived thickness values (eqs 1 and 2) are given in Table 2. The monolayer thickness, d_1, is almost identical to the nominal molecular length (within the experimental error), suggesting a tilt angle of the molecules with respect to the surface normal of, at most, 15°. The thickness derived from ellipsometry, which should be compared with $d_1 + d_2$, fits reasonably well with the XPS data. No significant difference is found between the thickness of the overlayers on *n*- and p-type GaAs.

This small molecular tilt is in contrast with previously reported values of 50−60°,[14,15,17] but is in agreement with a recent study.[19] It is also consistent with our FTIR data (i.e., lower antisymmetric stretch frequencies of the methylene groups compared to those in ref 14), supporting the high density of our monolayers.

The overall thickness of the interface layer, d_2 (∼2d_2*), ∼4 ± 1 Å, does not depend strongly on the molecular length (except for the case of C12). This value is smaller than previously reported values.[15,16] Moreover, because XPS, FTIR, contact angle and ellipsometry all suggest that we have a dense monolayer, we propose that a significant part of the detected

oxygen is incorporated between the organic molecules, forming a hybrid and a relatively stable interface together with the S atoms (see Figure 2).

As an additional reference, Table 2 presents a sample after prolonged (3 days) exposure to air. This sample shows a higher extent and degree of substrate oxidation, accompanied by a pronounced reduction in C and S intensities. This suggests that oxidation progresses via the formation of islands and the replacement of alkanethiols. The shorter (and less ordered) the monolayer is, the faster the process. For the layer that is most oxidized (C12; cf. Figure 3c), the signal for As−O (in addition to the Ga−O) is also seen.

In summary, both the contact angle and the FTIR measurements indicate that the C14, C16, and C18 monolayers are very dense, and, from the XPS measurement, it is evident that the amount of oxide in those samples is small. Thus, we conclude that these molecules form high-quality overlayers, with only a few sites left open for reaction with oxygen and water. In contrast, the C12 monolayer is less dense than the longer chain monolayers and thus undergoes faster substrate oxidation.

On the basis of all the measurements presented above, we conclude that these alkyl monolayers on GaAs are of sufficient quality to be studied in metal−insulator−semiconductor (MIS) junctions, with alkyl chains as the insulator and mercury (Hg) as the metal electrode. Following the characterization results, only the C14, C16, and C18 monolayers will be used to reliably determine the electronic structure of the junctions, while the C12 monolayer will serve as a reference.

4. *n*-GaAs/Molecules/Hg Junctions

4.1. Results of *J−V* Measurements. Figure 4b shows the *J−V* characteristics of *n*-GaAs−alkylthiol−Hg junctions in the reverse (a) and forward (b) bias regimes. Generally, all junctions are strongly rectifying. The shorter the molecules, the higher the current at a given voltage, in accord with the fact that these measurements reflect the structure of MIS junctions that are very similar except for the width of the insulating layer. In reverse bias, regardless of the high noise level, the slope of the curves decreases as the length of the molecules increases, consistent with the better blocking behavior for thicker monolayers at the interface (Figure 4a). The *J−V* curves at forward bias reveal a change in the (linear) slope at ∼0.4 V. Below this voltage, the curves have different slopes, while, above it, they are fairly parallel. This behavior is akin to what was observed recently for alkyl monolayers on Si.[5] It is also clear from Figure 4b that the *J−V* characteristics of the junction with the C12 monolayer at high bias are very different from those of the junctions with longer chains, and show nonlinearity and saturation in the high bias regime. This behavior is attributed to the relatively high oxide density at the C12/GaAs interface and to the lower density of the C12 monolayer. Thus, the *J−V* characteristics become a sensitive tool for determining the quality of the monolayer.

Quantitative analysis of the *J−V* data can be carried out using either the formalism of thermionic emission over a barrier in the semiconductor, or that of tunneling through an insulator film, as described in the next two sections. These two views are merged into a coherent model in section 4.4.

4.2. Thermionic Emission Analysis. Transport across metal−semiconductor junctions is described commonly by the thermionic emission−diffusion model[34] (Schottky model):

$$J \propto \exp\left(-\frac{q(n\Phi_{\mathrm{b}} - V)}{nkT}\right) \quad (3)$$
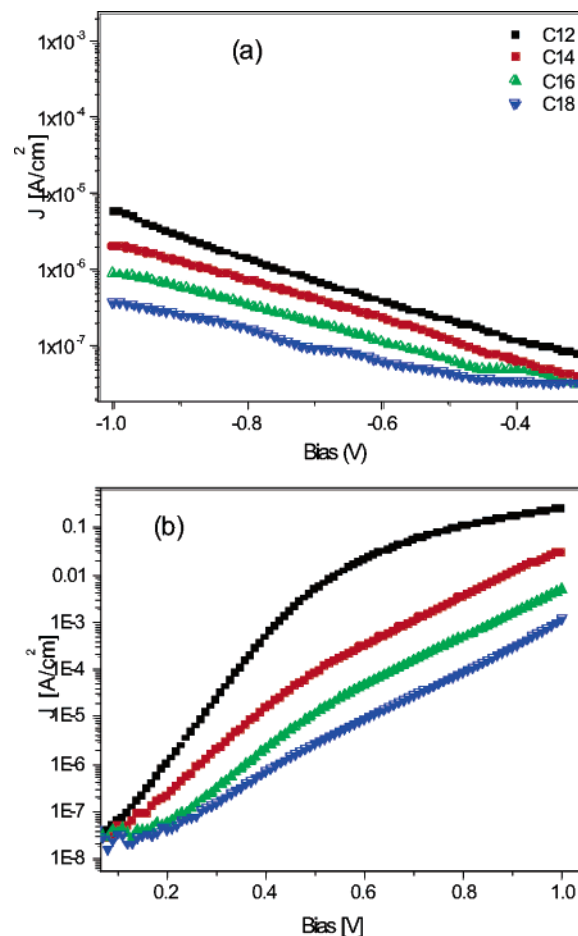
Figure 4. Experimental *J−V* curves for *n*-GaAs−S−C$_n$H$_{2n+1}$ ‖ Hg junctions (*n* = 12, 14, 16, and 18) in the reverse (a) and forward (b) bias regimes. C12: black rectangles; C14: red circles; C16: green upward pointing triangles; C18: blue downward pointing triangles. The current density is shown as a function of the applied bias. Curves are the average of ∼30 junctions. The error is 10%. The reverse bias data are smoothed by averaging over the nearest five points.

where *J* is the measured current density, *q* is the electron charge, *k* is the Boltzmann constant, *T* is the temperature, *n* is the ideality factor of the junction, and Φ_{b} is the electric potential barrier in the space charge region on the semiconductor side of the junction.

The *J−V* curves across *n*-GaAs−alkylthiol−Hg junctions at room temperature can be well described by the thermionic emission model; however, the fit should be separated into low and high bias regimes, with a crossover at 0.4 V (the "kink" in Figure 4b). The strong asymmetry of the *n*-GaAs curves (Figure 4a) is consistent with the rectifying regime of transport over a Schottky barrier, in contrast with the *p*-GaAs data, which are rather symmetric (cf. Figure 7, below). The extracted effective potential barrier in the semiconductor and the ideality factor for the different junctions are given in Table 3 for both regimes.

For MIS junctions, a modified version of the thermionic emission model predicts that the effective barrier height (extracted from eq 3) will depend on the tunneling distance in the following manner:[35,36]

$$\Phi_{\mathrm{eff}} = \Phi_{\mathrm{b}} + \frac{kT}{q}\beta d \quad (4)$$

where *d* is the tunneling distance, β is the attenuation factor, and the other symbols are defined above. Table 3 shows that, for the low bias regime, all the curves have the same potential

TABLE 3: Barrier Heights (Φ_b) and Ideality Factors (n), Extracted from the Current−Voltage Data of GaAs−S−C$_n$H$_{2n+1}$ ‖ Hg Junctions, for n = 12, 14, 16, and 18

monolayer	Φ_b (low bias) ±0.02 eV	n (low bias) ±0.1	Φ_b (high bias) ±0.02 eV	n (high bias) ±0.1
C12	0.85	1.3		
C14	0.86	1.8	0.74	3.3
C16	0.89	2.1	0.78	3.4
C18	0.88	2.6	0.83	3.4

barrier, unaffected by the monolayer thickness, in contrast with what is predicted by eq 4. Note that the ideality factor in the low bias regime varies with the molecular length. In contrast with what is found at low bias, eq 4 can explain the trend in the effective barrier height extracted at the high bias regime.

From a plot of Φ_{eff} versus d, we find $\beta = 0.8 \pm 0.3$ Å^{-1}. The intercept of the Φ_{eff} versus d plot yields $\Phi_b = 0.45 \pm 0.10$. This value is significantly less than the low bias barrier (Table 3, left), but is in agreement with general semiconductor theory,[34] which predicts reduced band bending at forward bias.

4.3. Tunneling View. The extremely high n values (high bias, Table 3) of the high-bias data show that the thermionic emission−diffusion model cannot be applied at high bias. In the high-bias regime, band bending is reduced, and tunneling across the insulator becomes the main process that limits transport. We can then analyze the data in that regime using, as a first approximation, the Simmons model[37,38] for tunneling through a rectangular barrier.

In this model, which is derived from the well-known Wentzel−Kramers−Brillouin (WKB) approximation for tunneling through an insulator, the transmission probability through the barrier depends exponentially on d, the tunneling distance, and the attenuation factor β:[35]

$$J = J_0 \exp(-\beta d) \tag{5}$$

where β depends on the applied bias:

$$\beta = 2\sqrt{\frac{2m^*\left(\Phi_t - \frac{qV}{2}\right)}{\hbar^2}} \tag{6}$$

Here, m^* is the effective mass of the electron for the tunneling process, $\hbar$ is Planck's constant, and Φ_t is the potential barrier for tunneling.

Such analysis for the high bias regime is shown in Figure 5. Notwithstanding large error bars, the dependence of β^2 on V shows a clear linear trend. From the slope and the intercept, we can deduce a tunneling barrier $\Phi_t = 0.8 \pm 0.3$ eV and an effective mass $m^* = 1.5 \pm 0.3 m_e$, where m_e is the free electron mass. This effective mass value is very different from those found experimentally for alkyl monolayers on Au[9] or on Si,[5] as well as those from theoretical predictions.[39] We can suggest that this very different effective mass is either connected with specific interactions between the alkyl chain states and the GaAs states or reflects the effect of the presence of oxide at the interface, which may decouple the molecular monolayer states from the semiconductor ones.

The values of the effective mass and the tunneling barrier have large errors because of the multiple steps needed to extract them. In addition, these values come from a very simple model that does not take into account the barrier shape and the asymmetry of the junction. Adding an independent measurement
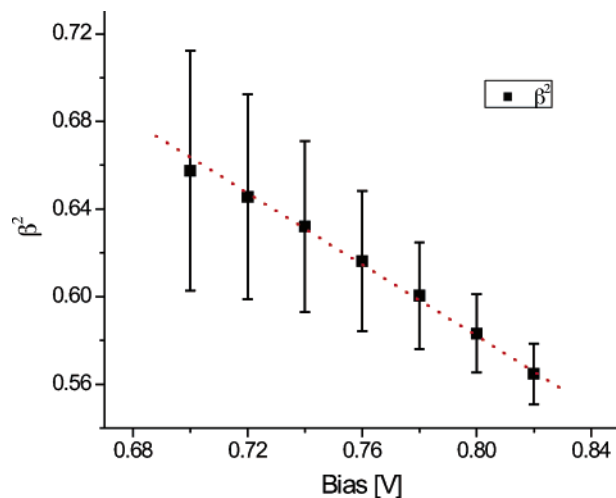
Figure 5. Plot of β^2 vs forward bias voltage (cf. eq 6 in text) for the GaAs−S−C$_n$H$_{2n+1}$ ‖ Hg junctions, as derived from the data shown in Figure 4 and using eq 6. The dotted line shows the best linear fit.

is therefore desirable to verify and, possibly, reduce the error in the values of m^* and Φ_t.

4.4. Rate-Limiting Step. The major characteristics of the transport across these molecular MIS junctions are the change in mechanism at ∼0.4 V (clearest for C12 and nearly invisible for C18) and the length dependence of the ideality factor, in contrast with the expected effect on the effective barrier height. To explain this behavior, we consider our system to be a coupled two-barrier model, where the barriers are the Schottky barrier inside the semiconductor and the barrier for tunneling through the molecular layer.

In the low bias regime, the Schottky barrier is the one that dominates the current transport, and the small changes in monolayer thickness do not play a significant role. Since the dipole of the molecules hardly changes for the range of molecular lengths used here, there is no significant change in the effective potential barrier. However, the ideality factor n clearly increases with increasing monolayer thickness. Since n is a measure of the efficiency of carrier transmission through the semiconductor interface,[40−42] we could argue that the monolayer thickness at the GaAs surface affects the efficiency of the transmission. This also implies that the two processes, that is, transport over the Schottky barrier and transport through the tunnel barrier, are not completely decoupled in this case, in contrast with previous findings with n-Si, where the ideality factor derived from the low voltage parts of the $J−V$ curves did not change upon increasing monolayer thickness.[5]

To explain this phenomenon, we view transport through these two adjacent regions as *dependent* (equilibrium) processes, coupled by the common current flowing across them. We attribute characteristic currents, J_{sc} and J_{ml} to semiconductor thermionic emission (section 4.2) and monolayer tunneling (section 4.3) transport. Actually, we can treat these currents as reaction rate constants (i.e., k_{sc} and k_{ml}), where the reaction is electron transport from one side of the junction to the other side. We write the overall reaction for such a process as[43−45]

$$A \xrightarrow{k_{sc}} A^* \xrightarrow{k_{ml}} B \tag{7}$$

(Note that, because the current is the rate of electron flow, this process can be likened to the Lindemann−Hinshelwood pseudo-unimolecular chemical reaction mechanism[43−45], A → A* → B). The ratio k_{sc}/k_{ml} is the main parameter here. If $k_{sc}/k_{ml} \ll 1$, the rate of charge transport through the semiconductor, J_{sc}, will

Electron Transport in GaAs−S−C$_n$H$_{2n+1}$−Hg Junctions

J. Phys. Chem. B, Vol. 110, No. 29, 2006 **14369**

control the transport. If $k_{sc}/k_{ml} \gg 1$, the rate of charge transport through the insulating layer, J_{ml}, will dominate. But, if k_{sc} and k_{ml} are comparable, the measured current will be, to a significant extent, limited by both rates. As a characteristic measure for the semiconductor limiting current, we take $J(0)$, the extrapolated current at 0 V, derived from the $\ln(J)$ versus V plots shown in Figure 4b, while the characteristic limiting tunnel current through the monolayer is $\exp(-\beta(0)d)$, where $\beta(0)$ is extrapolated from Figure 5 below. In the case of the n-GaAs−S−C18/Hg junction, the analysis of the experimental J−V curves shows

$$\frac{J_{sc}}{J_{ml}}\left(\propto \frac{J(0)}{\exp(-\beta(0)d)}\right) \cong 700 \qquad (8)$$

Only if $J_{sc}/J_{ml} = 0.1-100$ do we have a transition regime; therefore, this result implies that the rate of transport through the monolayer is the limiting one. Indeed, even though the value of 700 is extracted at 0 V, with tunneling as the dominant mechanism already there, we do not see a change in the J−V from thermionic emission- to tunneling-dominated behavior for the C18 junction, in contrast with what is the case for the other junctions. J_{sc}/J_{ml} values for the C16, C14, and C12 monolayers are 70, 3, and 0.01, respectively, and, with those monolayers, we can see the transition between the two mechanisms in the J−V curves as J_{sc} and J_{ml} become comparable with increasing bias.

In contrast with what we found for the n-Si alkyl system, here, at low bias, the J−V curves for the junctions with different molecular length monolayers do not coincide. The reason is that, even at low bias, there is a pronounced effect of tunneling. If the curves are nevertheless analyzed using the thermionic emission formalism, then this tunnel contribution leads to high ideality factors. These junctions are, thus, different from those made with n-Si, where all monolayers exhibit the same ideality factor (1.3) and J_{sc}/J_{ml} values that are similar and less than 0.01.

An alternative way to view the same physics is by monitoring the changes in monolayer thickness. The increase in the ideality factor (low bias, Table 3) may arise from the fact that the alkyl monolayers on GaAs are several angstroms thicker than their counterparts on Si (in terms of CH$_2$ units) because of the bridging S atom and the higher surface roughness of GaAs compared to that of Si. Simulations by Green et al.[13] of general MIS junctions showed that the J−V characteristics at low bias are independent of the insulator thickness as long as the thickness is less than some critical value, d_{cr}. For Si−insulator−Al, $d_{cr} = 28$ Å in the simulation. Assuming that the critical thickness for GaAs is similar to that for the Si−insulator−Al system, we have a similar situation here, because the total overlayer thickness exceeds this critical value for C16 and C18 if we add the extra thickness due to oxide and the S-binding group. Hence, both the slope of the J−V curves and the intercept vary with the thickness. According to the MIS model, increasing the molecular length (over Si) up to 24 carbons (with $\beta = 0.65$ Å^{-1}) will bring the system to d_{cr}, and $J_{sc}/J_{ml} \sim 1$. Thus, only at the limit of long alkyl chains can we expect to observe a tunneling contribution to the thermionic emission regime.

4.5. UPS Measurements. The independent measurement referred to at the end of section 4.3 is provided by UPS and IPES measurements[46] of the highest occupied and lowest unoccupied states of the GaAs/monolayer system (without second contact). It is clear that the top contact (Hg in the present case) changes the electronic structure of the system,[47] particularly the band bending in the semiconductor. However, since
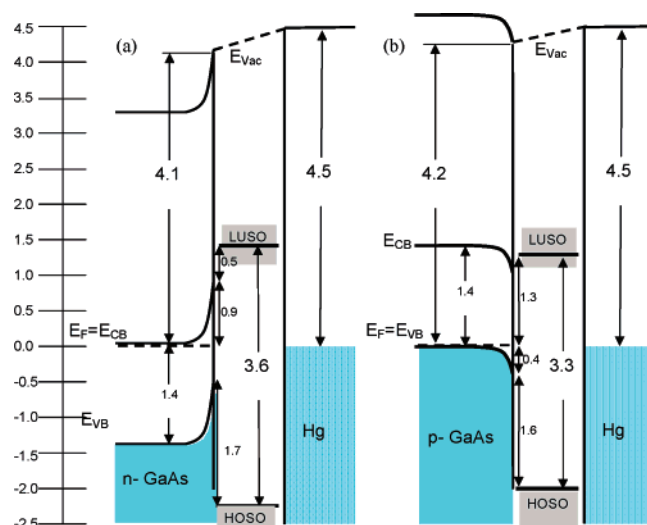
Figure 6. Proposed energy level and band diagrams for the GaAs−S−C$_{18}$H$_{37}$ ∥ Hg systems, based on experimental UPS, IPES, and I−V data for n-GaAs (a) and p-GaAs (b). The work function of the Hg is 4.5 eV, and the work functions for n- and p-GaAs are 4 and 4.2 eV, respectively. From UPS and XPS measurements, we find the band bending to be 0.9 eV for the n-type and 0.4 eV for the p-type. The highest occupied density of states at the interface was found to be ∼2.2 eV below the Fermi level for the n-type and 2 eV for the p-type GaAs, and the lowest unoccupied density of states at the interface was found to be ∼1.3−1.4 eV above the Fermi level for both the n-type and the p-type samples. Note that the unoccupied states start already below the bulk conduction band bottom for the p-type GaAs sample.

the molecules are attached chemically to the GaAs surface and only physically to the Hg electrode, most of the electronic nature of the junction, that is, the position of the molecular levels relative to the semiconductor band edges, should be captured by UPS and IPES on the free GaAs/alkyl surface. Given the very large gap between the alkyl-filled and empty molecular levels, here UPS and IPES measure composite semiconductor/molecule interface states, which we will call here the highest occupied system orbitals (HOSOs) and lowest unoccupied system orbitals (LUSOs). The onset of the LUSO measured by IPES is very close to the GaAs conduction band minimum and gives an approximate value of 1.4 ± 0.3 eV for the position of a large density of empty states above the Fermi level (E_F). The band bending (or the Schottky barrier, since the semiconductor is degenerate), measured by a combination of UPS and XPS (see Experimental Section), is $\Phi_b = 0.9 \pm 0.3$ eV, in fair agreement with the 0.85 eV Schottky barrier derived from the transport data. Adding the tunnel barrier yields a total barrier of $\Phi_b + \Phi_t = 1.65 \pm 0.4$ eV, in good agreement with the position of the empty states measured by IPES.

Figure 6a shows the proposed band diagram for the n-GaAs−S−C$_n$H$_{2n+1}$ ∥ Hg system. The band gap of GaAs is 1.4 eV, and, since the semiconductor is near-degenerate, the Fermi level in the bulk is essentially at the bottom of the conduction band. The onset of the filled states, presumably associated with the alkyl/GaAs interface, is difficult to pinpoint because the interface signal is considerably attenuated by the molecular monolayer. The HOSO position is found, from UPS measurements, to be ∼2.2 ± 0.3 eV below the Fermi level. This yields a HOSO−LUSO gap of approximately ∼3.6 ± 0.3 eV. This value is significantly less than the highest occupied molecular orbital (HOMO)−lowest unoccupied molecular orbital (LUMO) gap of the free alkyl chain, which is about 9−10 eV.[48]
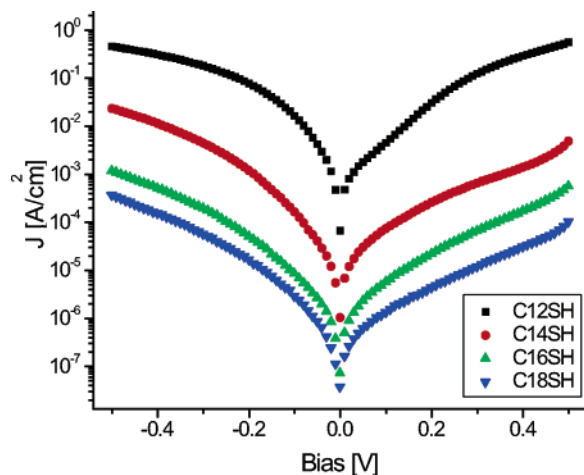
Figure 7. Experimental *I*−*V* curves for *p*-GaAs−S−C$_n$H$_{2n+1}$ || Hg junctions (*n* = 12, 14, 16, and 18). C12: black rectangles; C14: red circles; C16: green up triangles; C18: blue down triangles. The current density is shown as a function of the applied bias. Curves are the average of ∼30 junctions. The error is 10%.

5. *p*-GaAs/Molecules/Hg Junctions

An important difference between semiconductor/molecule and metal/molecule systems is that a change in dopant type or density changes the Fermi level position within the semiconductor band gap. This property provides another opportunity to understand transport properties because it allows for changing the energetics of the system without affecting the nature of the chemical bond. We therefore also study the same alkyl chains on *p*-GaAs. No significant differences in monolayer properties are observed between *n*- and *p*-GaAs, as seen by ellipsometry, contact angle, and XPS measurements.

5.1. *J*−*V* Measurements. The *J*−*V* curves for the *p*-GaAs/alkyl/Hg junctions are shown in Figure 7. The currents are 4 orders of magnitude smaller than those previously observed.[7] Forward and reverse characteristics are nearly symmetric, with a pronounced dependence on the number of carbons in the alkyl chains. Contrary to the results found with *n*-GaAs, only one distinct type of behavior is seen, which does not correspond to thermionic emission.[34] We will show that this behavior is well described by pure tunneling.

First, using eq 8, the ratio J_{sc}/J_{ml} is found to be larger than 200 for all the monolayers, which indicates that the bottleneck for transport is the monolayer and the limiting mechanism is tunneling. Second, using the Simmons model,[37,38] (eq 6) the tunnel barrier and effective mass are found to be $\Phi_t = 0.6 \pm 0.3$ eV and $m^* = 1.6 \pm 0.3 m_e$. This effective mass is the same as that obtained for *n*-GaAs, which suggests that the same carrier type is involved. To corroborate these findings, UPS and IPES measurements are performed on these samples.

5.2. UPS Measurements. Figure 6b shows the proposed band diagram for the *p*-GaAs−S−C$_n$H$_{2n+1}$ || Hg system. The HOSO−LUSO gap is 3.3±0.3 eV, which is almost the same as that for the n-type system, that is, again significantly larger than the alkyl HOMO−LUMO gap. There is no big change in the ionization energy, which means that the Fermi level is pinned, a situation often encountered for GaAs.[49] The band bending is 0.4 eV.

From IPES (see Figure 6b), we again find the onset of the unoccupied orbitals (LUSO) near the GaAs conduction band minimum and a large density of states at 1.3 ± 0.3 eV above the Fermi level, whereas significant densities of filled states start to appear deeper below E_F. This is consistent with the fact
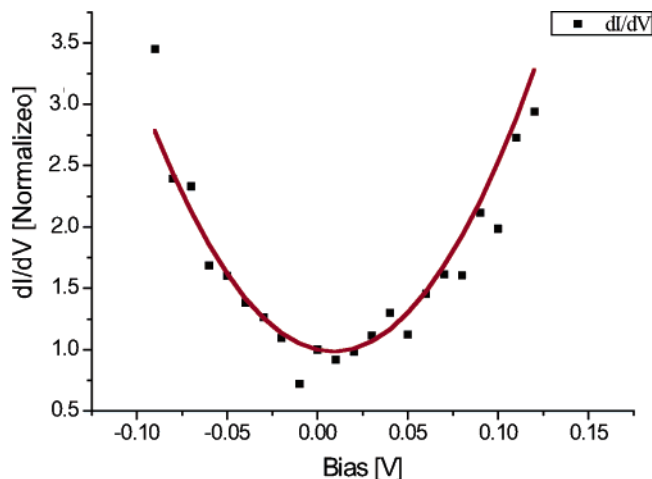
Figure 8. Conductance (d*I*/d*V*) of the *p*-GaAs−S−C$_{16}$H$_{33}$ || Hg junction vs the applied bias. The conductance (black squares) was calculated as the numerical derivative of the *I*−*V* curve for C16 that appears in Figure 7, normalized to the conductance at *V* = 0. The solid line (red) is the fit for the Brinkman model,[50] using a least mean squares fit. The tunneling barrier that can be extracted from this graph is $\Phi_t = 1.4$ eV.

that similar effective masses are derived from the Simmons model, as the empty states are again energetically more likely to be involved in the transport than the filled ones; that is, for both *n*- and *p*-GaAs, transport is probably dominated by electrons.

The LUSO value from IPES is too large to fit with the tunnel barrier obtained from the transport measurements. However, since we deal with near-degenerate *p*-GaAs, the conduction band of the bulk is actually at the same level or above the large density of the LUSO seen in IPES. As a matter of fact, the onset of the LUSO and conduction band minimum at the surface are so close that one can expect that new molecule/substrate interactions would take place. This may give rise to higher currents, which would appear in the Simmons model as a lower tunnel barrier.

5.3. Junction Asymmetry. In addition to this argument, we note that the Simmons model does not take into account the asymmetry of the junction. Yet, Figure 7 shows that the *J*−*V* curves are not completely symmetric. To check this, we use a model attributable to Brinkman et al.[50] for tunneling through asymmetric barriers. For barriers that are more than 10 Å thick, this model gives the following expression:

$$\frac{G(V)}{G(0)} = 1 - 0.1712\frac{d\Delta\varphi}{\Phi_t^{3/2}}V + 0.528\frac{d^2}{\Phi_t}V^2 \tag{9}$$

where $G(V)$ is the conductance (d*I*/d*V*) for every *V*, *d* is the monolayer thickness, Φ_t is the mean barrier for tunneling through the insulator (monolayer, in our case), and $\Delta\varphi$ is the energy difference between the two Fermi levels at the two sides of the insulator.

Using this expression for the data in the −0.15 < *V* < 0.15 bias range by taking the numerical derivative for the current, we find that $\Phi_t = 1.4 \pm 0.2$ eV, and the asymmetry is $\Delta\varphi = 14 \pm 10$ meV, averaged over different monolayers on *p*-GaAs. Figure 8 shows the normalized conductance, $G(v)/G(0)$, versus the bias and the least mean squares fit to the model that was used. The scatter in the plot can be understood by realizing that the *Y*-axis data were obtained by numerically determining the derivatives. However, after defining the thickness of the monolayer, φ is the only parameter that defines the shape of

Electron Transport in GaAs−S−C$_n$H$_{2n+1}$−Hg Junctions

J. Phys. Chem. B, Vol. 110, No. 29, 2006 **14371**

the conductance parabola. For our purpose, it suffices to show that the tunnel barrier extracted from this model is higher than the value obtained from the Simmons model and is indeed comparable with the value from the IPES measurement.

6. Conclusions

We have deduced electronic energy level diagrams for the *p/n*-GaAs−S−C$_n$H$_{2n+1}$ || Hg junctions, based both on electrical transport and spectroscopy. We find the effective mass of the carriers, as derived from the simple Simmons model for tunneling through a rectangular barrier, to be similar for both the *n*- and *p*-type junctions. Adding to this our knowledge of the positions for the highest occupied and lowest unoccupied system orbitals at the interface, that is, HOSO and LUSO, we conclude that the carriers playing the most important role in the transport properties of these junctions are the electrons, although there is a likely contribution of hole transport in the p-type GaAs system. (*Note added in proof*: We note that our reasoning for replacing the HOMO and LUMO concepts with HOSO and LUSO is somewhat similar to that used by Engelkes et al.[51] in their discussion of the inadequacies of the Simmons model.)

References and Notes

(1) Salomon, A.; Cahen, D.; Lindsay, S.; Tomfohr, J.; Engelkes, V. B.; Frisbie, C. D. *Adv. Mater.* **2003**, *15*, 1881 and references therein.

(2) Barraud, A.; Millie, P.; Yakimenko, I. *J. Chem. Phys.* **1996**, *105*, 6972.

(3) Aswal, D. K.; Lenfant, S.; Guerin, D.; Yakhmi, J. V.; Vuillaume, D. *Small* **2005**, *1*, 725.

(4) Liu, Y. J.; Yu, H. Z. *J. Phys. Chem. B* **2003**, *107*, 7803.

(5) Salomon, A.; Boecking, T.; Chan, C. K.; Amy, F.; Girshevitz, O.; Cahen, D.; Kahn, A. *Phys. Rev. Lett.* **2005**, *95*, 266807.

(6) J. Hsu, J. W. P.; Loo, Y. L.; Lang, D. V.; Rogers, J. A. *J. Vac. Sci. Technol. B* **2003**, *21*, 1928.

(7) Lodha, S.; Janes, D. B. *Appl. Phys. Lett.* **2004**, *85*, 2809.

(8) Vilan, A.; Ghabboun, J.; Cahen, D. *J. Phys. Chem. B* **2003**, *107*, 6360.

(9) Wang, W.; Lee, T.; Reed, M. A. *Phys. Rev. B* **2003**, *68*, 035416.

(10) Haick, H.; Ambrico, M.; Ligonzo, T.; Cahen, D. *Adv. Mater.* **2004**, *16*, 2145.

(11) Slowinsky, K.; Chamberlain, R.V.; Miller, C. J.; Majda, M. *J. Am. Chem. Soc.* **1997**, *119*, 11910.

(12) Holmlin, R. E.; Haag, R.; Chabinyc, M. I.; Ismagilov, R. F.; Cohen, A. E.; Terfort, A.; Rampi, M. A.; Whitesides, G. M. *J. Am. Chem. Soc.* **2001**, *123*, 5075.

(13) Green, M. A.; King, F. D.; Shewchun, J. *Solid-State Electron.* **1974**, *17*, 563.

(14) Sheen, C. W.; Shi, J. X.; Martensson, J.; Parikh, A. N.; Allara, D. L. *J. Am. Chem. Soc.* **1992**, *114*, 1514.

(15) Ye, S.; Li, G.; Noda, H.; Uosaki, K.; Osawa, M. *Surf. Sci.* **2003**, *529*, 163.

(16) Seker, F.; Meeker, K.; Kuech, T. F.; Ellis, A. B. *Chem. Rev.* **2000**, *100*, 2502.

(17) Zhang, Q.; Huang, H.; He, H.; Chen, H.; Shao, H.; Liu, Z. *Surf. Sci.* **1999**, *440*, 142.

(18) Remashan, K.; Bhat, K. N. *Thin Solid Films* **1999**, *342*, 20.

(19) McGuiness, C. L.; Shaporenko, A.; Mars, C. K.; Uppili, S.; Zharnikov, M.; Allara, D. L. *J. Am. Chem. Soc.* **2006**, *128*, 5231.

(20) Vilar, M. R.; El Beghdadi, J.; Debontridder, F.; Artzi, R.; Naaman, R.; Ferraria, A. M.; Botelho do Rego, A. M. *Surf. Interface Anal.* **2004**, *36*, 1783.

(21) Adlkofer, K.; Tanaka, M. *Langmuir* **2001**, *17*, 4267.

(22) Bryce, C.; Berk, D. *Ind. Eng. Chem. Res.* **1996**, *35*, 4464.

(23) Graf, D.; Grundner, M.; Ludecke, D.; Schulz, R. *J. Vac. Sci. Technol. A* **1990**, *8*, 1955.

(24) Wada, S.; Kasahara, F.; Hara A.; Ikoma, H. *Jpn. J. Appl. Phys.* **1998**, *37*, 427.

(25) Ishikawa, T.; Ikoma, H. *Jpn. J. Appl. Phys.* **1992**, *31*, 3981.

(26) Kim, J. W.; Kang, M. G.; Park, H. H *Thin Solid Films* **1999**, *355−356*, 423.

(27) Beerbom, M.; Henrion, O.; Klein, A.; Mayer, T.; Jaegermann, W. *Electrochim. Acta* **2000**, *45*, 4663.

(28) Lebedev, M. V.; Mayer, T.; Jaegermann, W. *Surf. Sci.* **2003**, *547*, 171.

(29) Briggs, D., Seah, M. P., Eds. *Practical Surface Analysis*, 2nd ed.; Wiley: New York, 1990; Vol. 1.

(30) Avci, R.; Cai, Q.; Lapeyre, G. J. *Rev. Sci. Instrum.* **1989**, *60*, 3643.

(31) Salomon, A.; Arad-Yellin, R.; Shanzer, A.; Karton, A.; Cahen, D. *J. Am. Chem. Soc.* **2004**, *126*, 11648.

(32) Allara, D. L.; Nuzzo, R. G. *Langmuir* **1985**, *1*, 52.

(33) The ~0.2 eV shift to lower binding energy after sputtering is attributed to a sputtering-induced change in the surface potential, a common feature in core and valence bands.

(34) Sze, S. M. *Physics of Semiconductor Devices*, 1st ed.; Wiley: New York, 1981.

(35) Cui, X. D.; Zarate, X.; Tomfohr, J.; Sankey, O. F.; Primak, A.; Moore, A. L.; Moore, T. A.; Gust, D.; Harris, G.; Lindsay, S. M. *Nanotechnology* **2002**, *13*, 5.

(36) Selzer, Y.; Salomon, A.; Cahen, D. *J. Phys. Chem. B* **2002**, *106*, 10432.

(37) Simmons, J. G. *J. Appl. Phys.* **1963**, *34*, 2581.

(38) Simmons, J. G. *J. Appl. Phys.* **1964**, *35*, 2655.

(39) Magoga, M.; Joachim, C. *Phys. Rev. B* **1999**, *59*, 16011.

(40) Mikhelashvili, V.; Eisenstein, G.; Garber, V.; Fainleib, S.; Bahir, G.; Ritter, D.; Orenstein, M.; Peer, A. *J. Appl. Phys.* **1999**, *85*, 6873.

(41) Card, H. C.; Rhoderick, E. H. *J. Phys. D: Appl. Phys.* **1971**, *4*, 1589.

(42) Fonash, S. J. *J. Appl. Phys.* **1975**, *46*, 1286.

(43) Lindemann, F. A. *Trans. Faraday Soc.* **1922**, *17*, 598.

(44) Hinshelwood, C. N. *Proc. R. Soc.* **1926**, *A113*, 230.

(45) Rice, O. K.; Ramsperger, H. C. *J. Am. Chem. Soc.* **1927**, *49*, 1617.

(46) Cahen, D.; Kahn, A. *Adv. Mater.* **2003**, *15*, 271.

(47) Tung, R. T. *Phys. Rev. Lett.* **1984**, *52*, 461.

(48) Tomsfohr, J. K.; Sankey, O. F. *Phys. Rev. B* **2002**, *65*, 245105.

(49) Ismail, A.; Palau, M.; Lassabatere, L. *J. Appl. Phys.* **1986**, *60*, 1730.

(50) Brinkman, W. F.; Dynes, R. C.; Rowell, J. M. *J. Appl. Phys.* **1970**, *41*, 1915.

(51) Englekes, V. B.; Beebe, J. M.; Frisbie, C. D. *J. Am. Chem. Soc.* **2004**, *126*, 14287.